DNA transistors switched by the Hofmeister effect

Tanner G. Hoog[1,†], Matthew R. Pawlak[1,†], Lauren M. Aufdembrink[1], Benjamin R. Bachan[1], Matthew B. Galles[3,4], Nicholas B. Bense[5], Katarzyna P. Adamala[1,2], Aaron E. Engelhart[1,2,*]

[1]Department of Genetics, Cell Biology, and Development, University of Minnesota, 6-160 Jackson Hall, 321 Church Street SE, Minneapolis, Minnesota 55455, United States

[2]Department of Biochemistry, Molecular Biology and Biophysics, University of Minnesota, 321 Church Street SE, Minneapolis, Minnesota 55455, United States

[3]GK Design Labs, LLC, 4401 Victoria Boulevard, Hampton, Virginia 23669, United States

[4]Structural Acoustics Branch, NASA Langley Research Center, Mail Stop 463, Hampton, Virginia 23681, United States

[5]NASA Glenn Research Center, 21000 Brookpark Road, Cleveland, Ohio 44135, United States

*e-mail: enge0213@umn.edu

[†]These authors contributed equally to this work.

Abstract

We are nearing the end of a remarkable period that began in the 1960s in which semiconductor manufacturers succeeded in shrinking die and feature sizes logarithmically, thus growing transistor counts exponentially with time. As we reach the theoretical physical limits of classical MOSFET semiconductors, DNA is a highly attractive candidate for future miniaturization of microprocessors. Here we show a foundational electronic device - a transistor - can be constructed from DNA. The nanodevice is comprised of two strands, one of which can be selectively switched between a G-quadruplex and duplex or single-stranded conformations. This switching ability arises from our discovery that perchlorate, a chaotropic Hofmeister ion, selectively destabilizes duplex over G-quadruplex DNA. By varying perchlorate concentration, we show that the device can be operated as a switch or signal amplifier. State switching can be achieved in three ways: thermally, by dilution, or by concentration. In each case, when operated in the presence of the cofactor hemin, the device catalyzes electron transfer in only the G-quadruplex state.

Background

In 1965, the co-founder of Intel, Gordon Moore, predicted a yearly doubling of the number of components per integrated circuit for the following ten years.[1] "Moore's Law" has held true beyond this period and throughout the computing era; transistor counts have grown exponentially with a doubling period of 1-2 years.[2] These doublings have been enabled by continuous miniaturization of semiconductors. The Intel 8008, released in 1972, was manufactured by a 10 micron (10,000 nm) process, and it contained 3,500 transistors.[3] The Apple A13, released in 2019, is manufactured by a 7 nm process in Samsung's foundry, and it contains 8,500,000,000 transistors.[4] The most advanced current commodity semiconductors are manufactured using this 7 nm process. At present, only two semiconductor manufacturers (Samsung and TSMC) possess foundries capable of shipping semiconductors produced using a 7 nm process.[5] These manufacturers plan to pursue a 3 nm process, and a consensus has not emerged whether further die shrinks will be possible.[6]

Biomolecules have been invoked by several groups as an attractive means of manufacturing semiconductors at smaller scales than will be possible with even the most advanced processes for MOSFET manufacturing. A range of techniques have been employed, including microbial systems, protein-directed assembly of metal clusters, metallated base pairs, and biopolymer-directed assembly of nanoparticles.[7–11] With 0.34 nm spacing between nucleobases and exquisite, atomic-precision self-assembly directed by nucleobase hydrogen bonding, nucleic acids are an especially attractive means by which to pursue further miniaturization of electronics. The phosphoramidite synthesis method by which the overwhelming majority of synthetic DNA is produced today allows for inclusion of essentially any chemical functionality, including redox-active side chains and alternative base pairs.[12] Furthermore, DNA can be prepared by biological means, enabling scale-up of manufacture in live-cell systems or systems employing cell-free lysate-based extracts.

DNA possesses inherent conductivity; a hole generated by a single-electron oxidation can propagate through a double helix. However, the utility of DNA as a general-purpose conductor is limited by the fact that each nucleobase possesses a different oxidation potential. As a result, a hole generated by single electron oxidation of DNA will migrate to a guanine, the most readily oxidized nucleobase, generating guanine radical cation, which in turn can undergo a range of chemical transformations, generating damage lesions such as 8-oxo-7,8-dihydroguanine and 2,5-diamino-4H-imidazol-4-one.[13] One means by which DNA can perform electron transfer and avoid such damage, enabling multiple turnover of electron transfer, is by employing a prosthetic group, as many enzymes that perform electron transfer in nature do. Hemin, one such prosthetic group, binds selectively to a noncanonical structure formed by G-rich sequences of DNA, termed a G-quadruplex, which activates it to perform electron transfer.[14–16] By binding hemin, the same prosthetic group employed by natural redox enzymes, such as peroxidases and Cytochrome P450s, DNA can perform electron transfer in a biomimetic fashion while mitigating the oxidative damage issues associated with attempting to use it as a classical conductor.[17]

Sequences of DNA and RNA that can exhibit either G-Quadruplex or non-G-quadruplex (e.g., unpaired or Watson-Crick base paired) structures depending on context are a ubiquitous feature of life. Similarly, living organisms actively remodel these structures.[18–20] A chemical system that enabled reversible, programmable structure switching would afford a powerful tool for dynamic electron transfer behavior in DNA nanostructures. We thus sought to develop a chemical system to switch the same DNA between secondary structure states, reasoning that this would combine the speed and repeated reversibility of pH-switchable DNA nanomotors with the compatibility with static pH observed in strand-exchange based systems.[21–26]

Base pairs have ca. one half the solvent-buried hydrophobic surface area of G-quartets, and Hofmeister ions exert their effects by interactions with the surface of biopolymers.[27] Similarly, G-quartets coordinate dehydrated ions, and high-salt solutions influence biopolymer folding by osmotic effects.[27,28] We thus reasoned that a DNA duplex and G-quadruplex would thus exhibit differential destabilization by chaotropes. Here, we demonstrate that perchlorate, a chaotropic anion that is ubiquitous in lithium-ion battery electrolytes, is a selective denaturant for duplex vs. quadruplex DNA. We have exploited this phenomenon to develop a molecular transistor made of DNA that can be switched between three states: a duplex, a G-Quadruplex, and a single-stranded state. We show that this switching can be performed thermally, by dilution, or by concentration. We show that the device can be switched over 100 times without degradation, and that it is also capable of performing signal amplification by binding hemin and catalyzing electron transfer in the G-Quadruplex state (**Figure 1**).

Results

Förster Resonance Energy Transfer (FRET) is a means of nonradiative energy transfer mediated by dipole-dipole coupling of two chromophores.[29] The r^6 distance dependence of this phenomenon affords exceptionally sensitive response to the structural state of the system in use, affording both a convenient means of monitoring secondary structure as well as a potential means of nanoscale optoelectronic coupling. We designed two FRET reporter systems, **G4-Dark** and **Duplex-Dark** (**Figure 2a-f** and **Table 1**)**,** to allow readout of their folding state. **G4-Dark** was comprised of equimolar amounts of **Fluorescein-G4-Quencher,** a DNA sequence that could form a G-Quadruplex, and **G4Comp**, its Watson-Crick complement. **Fluorescein-G4-Quencher** was 5′-labeled with a fluorescein tag and 3′-labeled with a quencher. Thus, this system would exhibit fluorescence when **Fluorescein-G4-Quencher** was either unfolded or hybridized to **G4Comp.** When **Fluorescein-G4-Quencher** was folded into a G-quadruplex, fluorophore and quencher would be brought into spatial proximity and quenched.

Duplex-Dark was comprised of equimolar amounts of strands of the same sequences as we employed in **G4-Dark** with rearranged reporters. **Fluorescein-G4,** a 5′-fluorophore-labeled sequence that could form a G-quadruplex, and **G4Comp-Quencher, a** 3′ quencher-labeled sequence. In this system, the fluorescein reporter exhibits fluorescence when **Fluorescein-G4** is either folded into a G-quadruplex or is unfolded. Upon hybridization of the two strands to form a double helix, this system would quench.

We first examined the thermal response of the **Duplex-Dark** system in $LiClO_4$ solution (conditions in which only duplex and unfolded states are possible, due to the stability trend in G-quadruplexes ($K^+ > Na^+ >>> Li^+$).[28]**. (Table 2**, **Figure 2g**, **Supplementary Figures 1-6**). At 100 mM $LiClO_4$, **Duplex-Dark** exhibited fluorescence response consistent with a double-stranded to unfolded structural transition at 79.8 °C (**Duplex-Dark** possesses adjacent reporters in the duplex state, resulting in a systematic slight elevation of T_M relative to other sequence-related systems with differing tags).[30] As the salt concentration was increased, the thermal midpoint initially increased to a maximum of 84.7 °C in 1 M $LiClO_4$, above which it decreased to a minimum of 46.6 °C in 4 M $LiClO_4$. This is consistent with electrostatic stabilization effects being predominant at lower salt concentrations and Hofmeister ion effects at higher concentration, as has been previously observed.[31]

We next examined the thermal response of the **Fluorescein-G4-Quencher** component of **G4-Dark** in $NaClO_4$-containing solution to ascertain the impact of this salt on the stability of the G-Quadruplex states of this system (**Figure 2h**, **Supplementary Figures 7-17**). In all $NaClO_4$-containing solutions, **Fluorescein-G4-Quencher** formed a G-Quadruplex, giving a 65.1 °C thermal midpoint in 100 mM $NaClO_4$; this temperature increased with increasing $NaClO_4$, consistent with the electrostatic screening afforded by Na^+ as well as its binding to the central channel within the G-quadruplex. Between 1-4 M $NaClO_4$, the G-Quadruplex was so stable it was not fully denatured, even at 95 °C (representative melting curve of 4M $NaClO_4$ in Figure 2h). In 5 M $NaClO_4$ and above, thermal midpoints were measurable and decreased with increasing perchlorate but remained high. Even in saturated $NaClO_4$ (ca. 9 M and containing less than three water molecules per ion), **Fluorescein-G4-Quencher** exhibited a higher thermal midpoint (73.7 °C) than in 100 mM $NaClO_4$ (65.1 °C).

The destabilization of the DNA duplex in **G4-Dark** and **Duplex-Dark** was marked (Figure **2i**) and exhibited a near-linear response in thermal midpoint of -7 °C/M $NaClO_4$ between 1 and 9 M (r^2=0.97); these duplexes exhibited thermal midpoints of ca. 75 °C at 100 mM $NaClO_4$ and 27-28 °C at 7-8 M $NaClO_4$. In contrast, perchlorate-induced destabilization of the G-Quadruplex formed by the G-rich strands was less pronounced and/or more than compensated by the presence of additional sodium (**Figure 2i**). **Fluorescein-G4-Quencher** exhibited a thermal midpoint of 65.1 °C at 100 mM $NaClO_4$ and 73.7 °C

in saturated sodium perchlorate (ca. 9 M). That is, in a polymorphic sequence, one possible secondary structure (dsDNA) that is *more* stable in low perchlorate than an alternative fold (a G-Quadruplex) becomes *less* stable than the alternative fold in high perchlorate.

Because of this, we speculated that **G4-Dark** could be thermally switched between all three states (duplex, G-Quadruplex, and single-stranded) at intermediate perchlorate concentrations. (**Figure 2j, Supplementary Figures 18-28**). Consistent with this, we observed a single transition at low (0.1 M) $NaClO_4$, which corresponded to the duplex-to-single-strand transition. At high $NaClO_4$ (saturated/ca. 9 M), we also observed a single transition, which corresponded to the G-Quadruplex to single-strand transition (**Figure 2j**), confirmed by the lack of thermal dequenching under these conditions with **Duplex-Dark** (**Figure 2k**).

We next sought to characterize the reversibility of cycling through the system's states. Reversibility without degradation is a requirement for a nanoelectronic device and a potential concern given some structure-switching nanodevices' propensity to exhibit degradation with repeated switching due to buildup of waste products.[22,24] To do so, we thermally cycled a sample of **G4-Dark** in 4 M $NaClO_4$ (conditions in which all three states are thermally accessible) 100 times while monitoring fluorescence. The sample did not exhibit degradation during this experiment (**Figure 3a-d)**.

Given the above, we reasoned that it would be possible to switch the state of our device from G-Quadruplex to duplex (by diluting it with aqueous buffer, lowering the concentration of perchlorate) or from duplex to G-Quadruplex (by removing water under vacuum, increasing the concentration of perchlorate). To do so, we performed dilutions of high-salt solutions of **G4-Dark** (which would initially exist in its dark state and transition to its light state) and **Duplex-Dark** (which would initially exist in its light state and transition to its dark state). **G4-Dark** recovered fluorescence upon dilution from 8 M to 0.8 M, and **Duplex-Dark** lost fluorescence following the same dilution (**Figure 3e**). Conversely, we sought to switch the system by removal of solvent. To do so, we took samples with an initial volume of 200 µL and initial concentration of 0.1 M $NaClO_4$ and placed them in a vacuum chamber. We monitored these samples by fluorescence imaging with a custom-built device (**Supplementary Figures 29-36**). The samples, initially in low $NaClO_4$, behaved as expected for the duplex state, with **G4-Dark** exhibiting fluorescence and **Duplex-Dark** in a dark state. **Duplex-Dark** remained dark during concentration while the fluorescence of **G4-Dark** gradually increased as the solution became more concentrated. Finally both solutions reached a critical concentration of $NaClO_4$ at which they transitioned to the G-quadruplex state and **Duplex-Dark** became fluorescent and **G4-Dark** became nonfluorescent (**Figure 3f-i, Supplementary Videos 1 and 2, Supplementary Code 1-3**).

G4-Dark and **Duplex-Dark** represent critical proofs of concept of a DNA transistor that operates via light output. A physical state change in the device results in enabling or disabling an energy transfer pathway in which one chromophore, upon absorbing a quantum of energy, transfers that energy *via* dipole-dipole coupling to another chromophore. These devices are analogous to an application of a transistor in which it is employed as a switch.

Another foundational application of transistors in electronics is their use to provide gain. To show this in our system we constructed **G4-Amplifier,** which was comprised of **G4Redox**, **G4Redox-Comp,** and the cofactor hemin activates hemin to promote electron transfer. We employed Amplex Red, a nonfluorescent dye that is oxidized to the fluorescent, red-colored pigment resorufin catalytically by the peroxidase formed between a G-quadruplex and hemin (**Figure 4a-c**).[32]

The potential difference in this system is defined by the concentration of terminal electron acceptor (hydrogen peroxide) and the redox chemistry of the probe. These are held constant between experiments, and so we determined gain of this system as the ratio of the rate of electron transfer performed by the G-Quadruplex/hemin complex compared to that performed by hemin alone (**Figure 4d**). This is analogous to the gain, h_{FE}, afforded by a transistor. In 0.1 and 5 M $NaClO_4$, the **G4-Redox** component of **G4-Amplifier** binds hemin and can perform electron transfer, with enhanced activity in 5 M relative to 0.1 M $NaClO_4$ (**Figure 4e, Supplementary Table 1, Supplementary Figures 37-40**). In saturated $NaClO_4$, electron transfer is suppressed due to lack of hemin-G quadruplex interactions.

In 0.1 M $NaClO_4$, **G4-Amplifier** exists entirely as a duplex, hemin binding is thus abrogated; resorufin was produced at < 30 nM/min when **G4-Amplifier** was present or when it was absent **(Figure 4f)**. In 5 M $NaClO_4$, **G4-Amplifier** dissociates into **G4Redox** folded into a G-Quadruplex, which is competent to bind hemin, and **G4Redox-Comp** exists as a single strand. The resulting hemin-**G4Redox** complex performs electron transfer (as measured by the reporter dye Amplex Red's conversion to resorufin) 35-fold more rapidly than hemin alone (**Supplementary Figures 37-39**). The hemin-**G4Redox** complex produced resorufin at 300 nM/min vs. unbound hemin, which produced it at 9 nM/min (i.e., a 35-fold gain, comparable to the h_{FE} of the 2N2369 transistor).[33] At still higher $NaClO_4$, hemin-G-quadruplex binding decreases, and in saturated (ca. 9 M) $NaClO_4$, resorufin was produced at a much lower rate of 46 nM/min. Thus, perchlorate concentration can be varied to switch the state of the DNA transistor as well as to modulate the gain of the device.

In order to demonstrate electron transfer could be thermally switched as well, we measured Amplex Red oxidation using **G4-Amplifier** in 4 M $NaClO_4$ (**Figure 4g**). At 20 °C, electron transfer was near-zero. As the sample was heated and switched from duplex to G-Quadruplex, the rate of electron transfer exhibited a significant increase, reaching a maximum at 60 °C and again decreasing as the G-Quadruplex unfolded. This is consistent with the thermal denaturation curve generated by monitoring A_{295} (a diagnostic wavelength for G-quadruplex formation) of this sample (**Supplementary Table 1**, **Supplementary Figures 41-42**). Notably, hydrogen peroxide was required. Perchlorate ion, despite its exceptionally high oxidation potential, did *not* suffice as an electron acceptor in this system, demonstrating the exceptional specificity afforded by biocatalyst-based electronic systems and the compatibility of this high-oxidation state ion that is ubiquitous in legacy electronic systems with biomolecular electronics.

Discussion, Conclusions, and Outlook

Here, we have demonstrated that a "soft" nanomaterial - DNA - can exhibit the essential functions of a transistor - switching and signal amplification. We also have shown that such a device be operated in the presence of high concentrations of perchlorate - typically considered too denaturing to support biopolymer secondary structures. Perchlorate and other weakly coordinating anions are ubiquitous in lithium-ion battery electrolytes at molar concentrations, similar to those used in this work.[34–36] This underscores the utility of our device in the harsher environments associated with semiconductors. As a period in which hybrid nanoelectronics perform computing tasks will likely be required as the transition from MOSFET-based electronics to next-generation technologies occurs, devices capable of functioning in such environments will be critical. The unique switchability characteristics of the device are well-suited for control by a number of semiconductor technologies, including thermal- (thermocouples/Peltier junction devices) and pressure-based (MEMS vacuum pumps) technologies, with the possibility of a thermal or vacuum domain of a device addressing a region of a chip at any given time. All these features promise to be of use in interfacing biopolymers with conventional electronics, as was recognized as a Key Technical Area by the Semiconductor Research Corporation in their Biocomputing Roadmap.[37]

Dual-labeled DNA strands containing FRET pairs are ubiquitous in modern biochemistry laboratories. As the tool of choice for real-time PCR detection, they are readily prepared to order by contract synthesis houses. At current prices (Integrated DNA Technologies, Coralville, IA), a typical dual-labeled probe costs ca. $300 for a guaranteed yield of on the order of 1 nmol, or ca. 10^{14} molecules of DNA. This represents ca. four orders of magnitude more strands of DNA, each capable of performing the transistor functions shown here, than transistors present in the Apple A13 Bionic processor manufactured by Samsung's 7 nm process.[4] Unlabeled strands (i.e., unmodified DNA), such as those used routinely as primers in PCR, or, in this work, for electron-transfer based signal amplification in **G4-Amplifier,** are more inexpensive still, with ca. 3 orders of magnitude higher yield at ca. 1 order of magnitude lower price.

We anticipate that optical couplings such as those we have shown can function in **G4-Dark** and **Duplex-Dark** could be employed in single-molecule, switchable nano-optoelectronic couplings. The level of structural diversity and atomic-scale addressability that is possible in nucleic acid synthesis is unparalleled by any other polymer. The essentially infinite tunability of dye wavelengths and chemistries, photochemically active and photochemically switchable monomers, and myriad of other chemical modifications make nucleic acids an exceptionally attractive platform for nanoelectronics.

Beyond this, the world's capabilities in nucleic acid synthesis are both broad, in sequence space – Twist Bioscience has made multiple agreements with Ginkgo Bioworks to synthesize DNA at the 10^8 bp scale – and deep, in scale-up capabilities – Agilent's oligonucleotide facility in Boulder, CO can produce oligonucleotides at the 1 *mole* per run scale and has yearly synthesis capacity on the order of 10^2 kg. This scale of synthesis was first achieved by Agilent in 2009 and amounts to on the order of 10^{24} individual strands of DNA per year (calculated based on a typical 25 nt oligonucleotide)[38]. Thus, even ten years ago, a single oligonucleotide manufacturer possessed the capacity to produce in one year oligonucleotides, of the size we have employed in this study, in numbers two orders of magnitude greater than the ca. 10^{22} MOS transistors fabricated by all semiconductor manufacturers globally between 1960 and 2018. Nucleic acids can also be produced at large scale in cell culture or cell-free enzymatic systems. The ability to prepare DNA by large-scale organic synthesis or biologically makes nucleic acid-based, synthetic biology approaches to nanoelectronics and data storage particularly appealing.

In the present system, duplex-to-quadruplex remodeling occurs due to a secondary structure-specific Hofmeister effect, reported here for the first time. Examples of secondary-structure remodeling are observed in life as well. Nucleic acids exhibit considerable polymorphism in biological systems, particularly in sequences that can form G-Quadruplexes. Such systems are diverse and widespread in biology and extend to both DNA and RNA, including proto-oncogene promoters,[39] the expansion segments of rRNA of higher organisms,[40–42] the rDNA corresponding to those expansion segments,[43], and eukaryotic messenger RNAs.[18,19]. Several proteins can remodel G-quadruplexes, and both energy-dependent (i.e., helicases) and energy-independent systems that can do so have been reported.[44,45]. ATP-dependent helicases are known to unwind G-quadruplex structures, and the RNA-binding protein Lin28 has been shown to unfold G-quadruplexes without the requirement for ATP.[44] The structure switching performed by Hofmeister ions in this work amounts to a bioinspired means of performing such remodeling.

Given that such remodeling processes are also operative in Nature and that hemin-G-Quadruplex promoted electron transfer has been suggested as being physiologically relevant, we speculate that conditional hemin-G-quadruplex complexes are means by which cells could conditionally enable electron transfer. For example, ribosomes from the neurons of Alzheimer's Disease patients have been shown to contain more iron than those from healthy patients, and these ribosomes possess peroxidase activity.[46] Human ribosomes are known to be polymorphic, particularly in their G-rich expansion segments, some of which have been observed to lack electron density in EM maps.[40,47] Rarely, particles clearly exhibit extended conformations consistent with Watson-Crick base pairing, but these same sequences possess exceptionally high G-Quadruplex forming potential and form G-Quadruplexes in cell-free *in vitro* experiments.[42,43]

We suggest that conditionally folded G-Quadruplexes in cells could collaborate with hemin, producing a means by which cells can perform conditional electron transfer that is analogous to the phenomenon we have employed in this work. Such a phenomenon could be exploited both by extant life or in synthetic biological systems, and we speculate this could have enabled conditionally active forms of prebiotic electron transfer catalysts, which have attracted intense interest in recent years.[48–50]

Acknowledgements

Several figures in this manuscript were made using BioRender.com. We thank Loren Williams and George Perry for helpful discussions. The imaging apparatus used here was developed as part of the RockSat-C 2018 sounding rocket program, sponsored by the Colorado Space Grant Consortium and NASA Wallops; we thank the NASA PAXC team members for helpful discussions. This work was supported by NASA Contract 80NSSC18K1139 under the Center for Origin of Life (to A.E.E. and K.P.A.).

Author Contributions

A.E.E., K.P.A., T.G.H., and M.R.P. conceived the project. T.G.H., M.R.P., L.M.A., and B.R.B. performed experiments. L.M.A. contributed computer codes and analysis. M.B.G. performed CAD of the fluorescence imaging jig. N.B.B. fabricated and assembled the fluorescence imaging jig. A.E.E., K.P.A., T.G.H., and M.R.P. wrote the paper.

Competing Interests

The authors declare no competing interests.

Materials & Correspondence

Requests for materials and correspondence should be directed to A.E.E. (enge0213@umn.edu).

Methods

Nucleic Acids

Oligonucleotides were obtained from Integrated DNA Technologies (Coralville, IA) and used as received. Labeled strands were obtained with HPLC purification and unlabeled strands were obtained with standard desalting.

Table 1. Sequences employed in this study.

System/Strand	Sequence
G4-Dark	
Fluorescein-G4-Quencher	6-FAM-TG GGT TAG GGA ATT CGG GTT AGG G-Iowa Black FQ
G4Comp	CCC TAA CCC GAA TTC CCT AAC CCA
Duplex-Dark	
Fluorescein-G4	6-FAM-TG GGT TAG GGA ATT CGG GTT AGG G
G4Comp-Quencher	CCC TAA CCC GAA TTC CCT AAC CCA-Iowa Black FQ
G4-Amplifier	
G4Redox	GGG TAG GGC GGG TTG GGA
G4Redox-Comp	TCC CAA CCC GCC CTA CCC

DNA Sample Preparation

Oligonucleotides were annealed in a T100 thermal cycler (Bio-Rad) by incubating at 95 °C for 2 minutes, then decreasing the temperature by 10 °C steps and annealing at each step for 1 minute to a final temperature of 25 °C. Except where otherwise specified, experiments were performed in 50 mM Li-HEPES, pH 7.4, with 1 µM of the duplexed or single stranded oligonucleotides.

Fluorescence-Monitored Experiments

Fluorescence measurements were performed using a Gemini XS plate reader (Molecular Devices) or a Cary Eclipse (Varian Technologies) fluorometer equipped with a thermostated peltier holder (Agilent Technologies) when bidirectional temperature control was required. Excitation was performed at 495 nm and emission was monitored at 520 nm.

For thermal denaturation studies, the sample was ramped from 20 °C to 95 °C (two heat/cool cycles) at 5 °C/min. Selected measurements were also performed with a slower 0.5 °C/min ramp rate to mitigate hysteresis. Thermal midpoints are reported as a sigmoid fit of the transition(s) in the second heating trace of two temperature ramps.

UV-Vis Monitored Experiments

Thermal denaturation experiments were performed using a qCHANGER 6/Cary60 (Quantum Northwest) interfaced to a Cary 60 UV-Visible spectrophotometer (Agilent Technologies) using a custom ADL script developed by Quantum Northwest to collect full spectra at each temperature as described previously. Heat sinking for the Peltier device was provided by a EXT-440CU ambient liquid cooling system (Koolance). Duplex melting transitions were monitored using the 260 nm trace from these datasets and G-Quadruplex melting temperatures were monitored using the 295 nm trace.

Amplex Red experiments (described further below) were monitored on a Cary 60 UV-vis (Agilent Technologies) or a SpectraMAX 340PC plate reader (Molecular Devices) with the PathCheck functionality enabled.

Fluorescence Imaging Under Vacuum

Samples were pipetted into PCR tubes with the lids open, which were inserted into a 3D-printed jig that was placed inside a black box. The jig was fabricated in PLA on a Prusa 3D printer. The box and its contents were placed in a vacuum desiccator (Supplementary Figures 29-36) and the chamber was continuously evacuated with a diaphragm pump (Welch 2014B-01). The samples were excited with LEDs with emission centered at 462-465 nm (Item B01GDO9UNY, Amazon). The samples were imaged with a camera (Raspberry Pi Module V2, Amazon) fixed at 90° relative to the light sources. A 12.5 mm longpass filter (Schott OG 550, Edmund Optics) was affixed with polyvinyl acetate adhesive (Elmer's Glue-All, Costco Wholesale) directly in front of the camera lens to block excitation light and pass emitted light. The camera was interfaced to a Raspberry Pi B+ (Amazon). A Python script controlled the Raspberry Pi's GPIO pins to illuminate samples at 1-minute intervals, collect images, and measured and plotted fluorescence intensity vs. time. Time-lapse movies were generated from captured images using FFmpeg.

Samples were prepared with a starting volume of 200 µL and 0.1 µM of **G4-Dark, Duplex-Dark,** or **Fluorophore-G4-Quencher** in 5 mM Li-HEPES, pH 7.4 and 0.8 M $NaClO_4$. After desiccation, the final volume was 20 µL with 50 mM Li-HEPES, 8 M $NaClO_4$ and 1 µM **G4-Dark, Duplex-Dark,** or **Fluorophore-G4-Quencher.**.

Electron Transfer Assay

Samples contained **G4-Amplifier** (i.e., **G4Redox** and **G4Redox-Comp**), **G4Redox** alone, or no oligonucleotide. G4Redox, when present, was at 1 µM and G4Comp, when present, was at 2 µM to ensure full duplex state at low perchlorate/temperature and that electron transfer catalysis observed was due to the G-Quadruplex state of **G4-Amplifier** and not residual unduplexed **G4Redox**.. The buffer used here was 5 mM sodium phosphate, pH 7.4 with varying sodium perchlorate concentrations. To initiate the reaction, hemin was added to a final concentration of 1 µM, hydrogen peroxide was added to a final concentration of 300 µM, and Amplex Red was added to a final concentration of 200 µM. Reactions were monitored by measuring the absorbance of resorufin at 570 nm. For the Cary 60 thermal activation-Amplex red assay, Amplex Red was added to a final concentration of 2 mM. All reactions contained 2% DMSO, which came from the hemin and Amplex Red stocks.

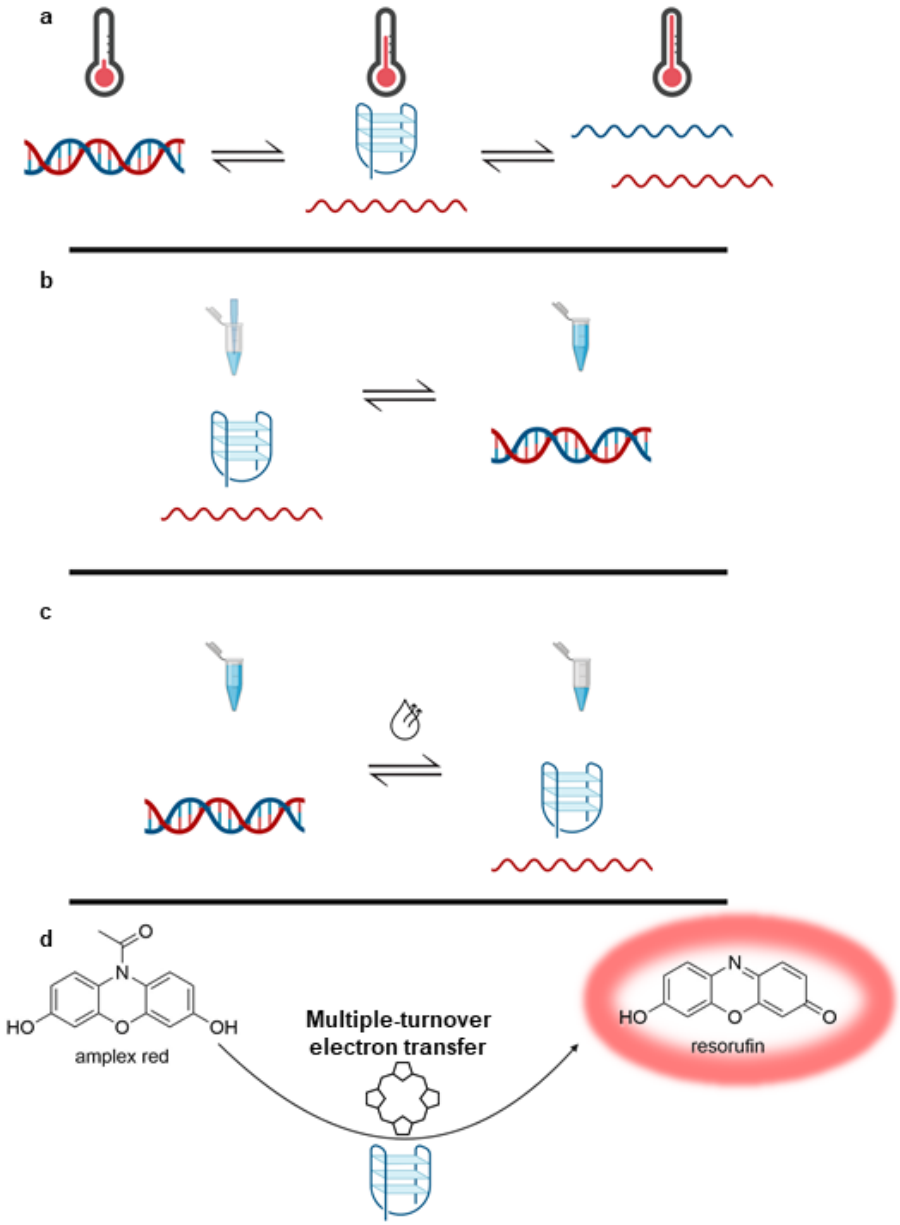

Figure 1. Mechanisms of switching the transistor: thermally (panel **a**), by dilution (panel **b**), and by concentration (panel **c**). In intermediate perchlorate concentrations, the transistor can be switched thermally (**a**) through three states. At low temperatures (left), it exists as a duplex; at intermediate temperatures, it exists as a G-quadruplex (center); and at high temperatures, it is single-stranded (right). At high perchlorate concentrations, it exists in only two states - only the G-quadruplex (center) and single-stranded (right) states. The transistor can also be switched between two states by varying concentration. In high-perchlorate solution, the device exists as a G-quadruplex, while in low-perchlorate solution, it forms a duplex. Thus, by diluting a high-salt solution (panel **b**), the device can be switched from a G-quadruplex to a duplex; and by removal of water from a low-salt solution (panel **c**), the device can be switched from a duplex to a G-quadruplex. In each case, the G-quadruplex form of the transistor is competent to perform signal amplification by catalyzing multiple-turnover electron transfer in the presence of hemin (panel **d** and Figure 4).

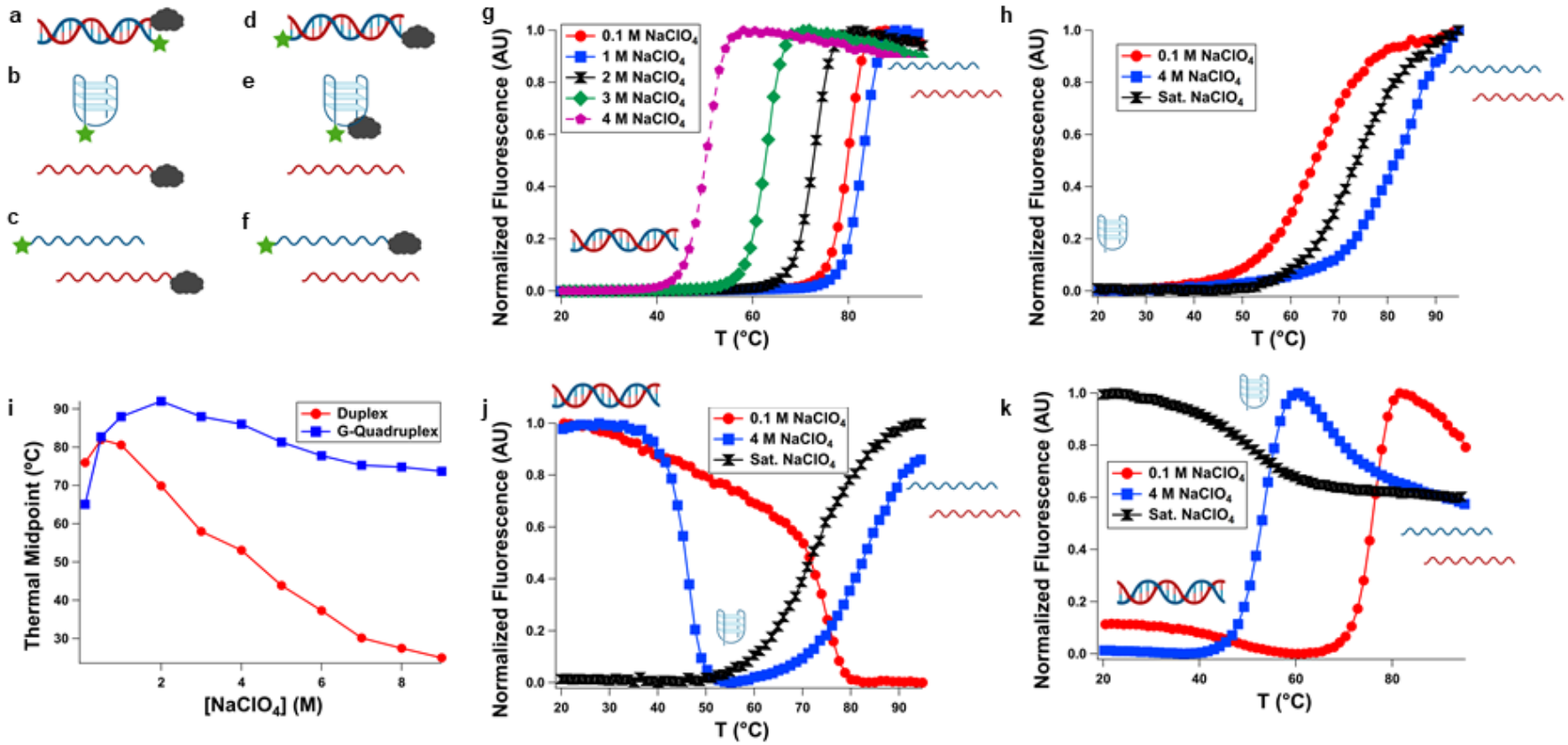

Figure 2. Systems employed in fluorescence-monitored thermal denaturation experiments (panels **a-f**). **Duplex-Dark** (panels **a-c**) consists of a 5′-fluorescein labeled strand (green star) and a 3′-Iowa Black FQ (grey cloud) strand and can exist in three states: A quenched duplex (**a**), a dequenched G-quadruplex and single strand (**b**), and a dequenched set of two single strands (**c**). **G4-Dark** (panels **d-f**) consists of a dual-labeled (5′-fluorescein, 3′-Iowa Black FQ) strand and its complement and can also exist in three states: A dequenched duplex (**d**), a quenched G-quadruplex and single strand (**e**), and a dequenched set of two single strands (**f**). When **Duplex-Dark** is operated in $LiClO_4$ solution, only duplex and single-stranded states are accessible. This transition is destabilized with increasing perchlorate (panel **g**). When only the **Fluorescein-G4-Quencher** component of **G4-Dark** is operated in $NaClO_4$ solution (panel **h)**, the G-Quadruplex-forming strand is significantly less destabilized by perchlorate (panel **i**), in contrast to the duplex, which exhibits ca. linear destabilization with increasing $NaClO_4$ concentration above 1 M (panel **i**). As a result of this differential stability, **G4-Dark** and **Duplex-Dark** can be switched thermally between duplex, G-quadruplex, and single-stranded states, and the temperatures at which these transitions occur can be tuned by varying the concentration of $NaClO_4$. In low perchlorate (0.1 M,

panels **j** and **k**), only the duplex-to-single stranded transition is observed (red circles). In intermediate perchlorate (4 M), the device transitions between duplex (at low temperature), G-Quadruplex (at intermediate temperature), and single-stranded (at high temperature) states (blue squares). In high perchlorate (saturated, ca. 9 M), the device exists only in the G-quadruplex and single-stranded states (black hourglasses).

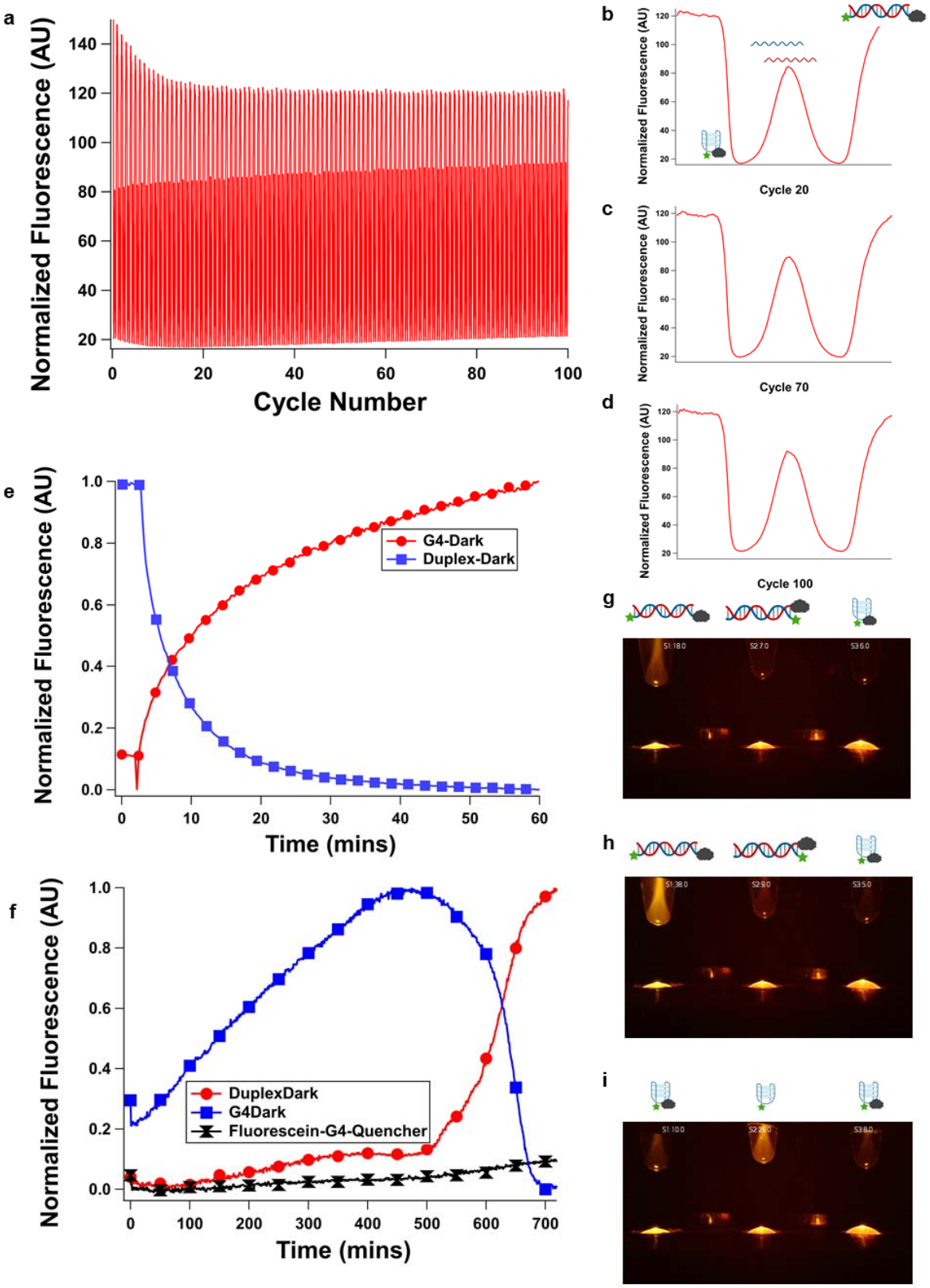

Figure 3. Switching behavior of **G4-Dark**. **G4-Dark** (which reports on all three states) was switched thermally 100 times between duplex, G-Quadruplex, and single-stranded states with no decay of fluorescence signal following an initial 10-cycle "burn-in" (panel **a** shows the full series of switching events; panels **b-d** show cycles 20, 70 and 100). While thermal switching is rapid, a "latching" behavior with slower switching is possible with chemical switching, enabling a high level of temporal control of device switching. To demonstrate this, **G4-Dark** and **Duplex-Dark were** also switched chemically by dilution on slower timescales, enabling refolding from the G-Quadruplex to duplex state (panel **e**) and vacuum concentration, enabling refolding from the duplex to G-Quadruplex state. In vacuum experiments, **G4-Dark** (left) **Duplex-Dark** (center) and Fluorescein-G4-Quencher (right) were employed (panel **f** shows fluorescence quantitated from images, panels **g-i** show various timepoints, and this experiment is shown in Supplementary Videos 1 and 2). Under all conditions, Fluorescein-G4-Quencher remained a G-quadruplex and did not emit fluorescence. At low (0.8 M) $NaClO_4$, the duplex state was favored, resulting in **G4-Dark** emitting fluorescence and **Duplex-Dark** existing in a fluorescence-quenched state (panel **g**). At intermediate perchlorate concentrations during vacuum concentration, the fluorescence of **G4-Dark** increased due to an increase in oligonucleotide concentration but an insufficient increase in $NaClO_4$ concentration to induce a structure change; **G4-Dark** remained fluorescent and **Duplex-Dark** remained in a quenched state due to this (panel **h**). Finally, upon ca. 10-fold concentration (to ca. 8 M $NaClO_4$, meniscus demonstrating ca. 10-fold concentration from 200 to 20 µL visible) **G4-Dark** and **Duplex-Dark** assumed their G-Quadruplex states, causing **G4-Dark** to quench and **Duplex-Dark** to become fluorescent (panel **i**). Brightness was increased by 50% in panels **g-i** relative to captured images for visual clarity. Original images with plots of image-quantitated fluorescence and annotations are shown in Supplementary Videos 1 and 2.

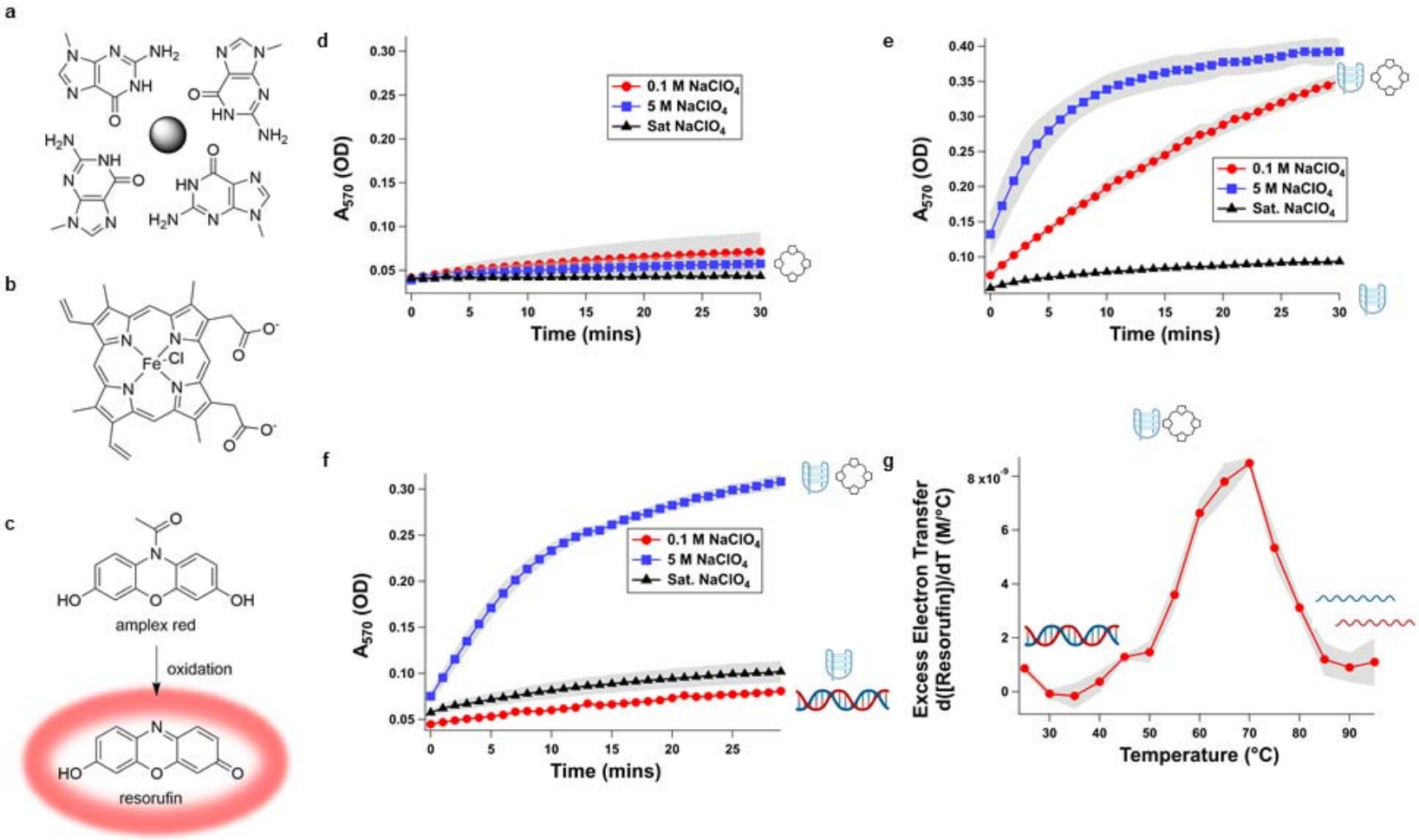

Figure 4. Switchable electron transfer amplification behavior of **G4-Amplifier** and its constituent components in the presence of hemin. When folded into the G-Quadruplex state, a solvent-exposed G-Quartet (panel **a**) is present which is known to provide a tight binding pocket for the

cofactor hemin (panel **b**); the complex formed by a G-Quadruplex and hemin can catalyze electron transfer. We visualize this here using the colorimetric electron transfer probe Amplex Red (panel **c,** top), which is initially colorless and nonfluorescent and, when oxidized, converts to the red fluorescent pigment resorufin (panel **c**, bottom). Hemin itself has a minimal background rate of electron transfer that is suppressed by increasing $NaClO_4$ concentration (panel **d**). When **G4-Redox** is operated as the only oligonucleotide constituent (i.e., under conditions in which the strand will form only a G-Quadruplex) in the presence of hemin, robust multiple-turnover electron transfer occurs in low (0.1 M, red circles) $NaClO_4$ solution, it is enhanced in moderate (5 M, blue squares) $NaClO_4$ solution, and it is suppressed in saturated $NaClO_4$ solution (black triangles) due to abrogation of hemin binding (panel **e**). When **G4-Amplifier** is operated in these same conditions, electron transfer is switched off in low (0.1 M) $NaClO_4$ solution due to duplex formation, switched on in moderate (5 M) $NaClO_4$ solution due to G-quadruplex formation with concomitant hemin binding, and switched off in saturated $NaClO_4$ solution due to abrogation of hemin binding (panel **f**). **G4-Amplifier** can also be switched thermally, exhibiting varying degrees of gain depending on its folding state. When ramped from 25 to 95 °C in 5 M $NaClO_4$ solution, excess electron transfer (as measured by rate of resorufin production in excess of that observed in hemin alone) starts at near-zero as the device exists in duplex form, increases substantially between 50 and 70 °C as the duplex melts and the G-Quadruplex forms, and it decreases again by ca. 90% between 70 and 90 °C as the G-Quadruplex unfolds and the single-stranded form of the device forms (panel **g**). These results are consistent with UV-visible monitored thermal measurements of secondary structures formed (Supplementary Figures 41 and 42).

Table 2. Thermal midpoints (°C) of **G4-Dark, Duplex-Dark,** and **Fluorescein-G4-Quencher** in $NaClO_4$ solution, and of **G4-Dark** and **Duplex-Dark** in $LiClO_4$ solution.

Strands/[ClO_4^-] (M)	0.1	0.5	1	2	3	4	5	6	7	8	Sat.
G4-Dark (**Fluorescein-G4-Quencher** and **G4Comp**)/$NaClO_4$	None[1] 73.9[2]	None[1] 77.4[2]	High[1,3] 73.8[2]	High[1,3] 66.7[2]	83.2[1] 48.8[2]	83.0[1] 45.6[2]	80.2[1] 37.0[2]	78.1[1] 32.2[2]	75.3[1] 27.0[2]	74.4[1] Low[2,4]	72.6[1] Low[2,4]
Duplex-Dark (**Fluorescein-G4** and **G4Comp-Quencher**)/$NaClO_4$	n/a[1] 75.9[2]	n/a[1] 82.0[2]	n/a[1] 80.5[2]	n/a[1] 69.9[2]	n/a[1] 58.2[2]	n/a[1] 53.1[2]	n/a[1] 43.9[2]	n/a[1] 37.3[2]	n/a[1] 30.3[2]	n/a[1] 27.6[2]	n/a[1] Low[2,4]
Fluorescein-G4-Quencher/$NaClO_4$	65.1[1] n/a[2]	82.7[1] n/a[2]	88[1,3] n/a[2]	92[1,3] n/a[2]	88[1,3] n/a[2]	86[1,3] n/a[2]	81.3[1] n/a[2]	77.8[1] n/a[2]	75.1[1] n/a[2]	74.9[1] n/a[2]	73.7[1] n/a[2]
G4-Dark (**Fluorescein-G4-Quencher** and **G4Comp**)/$LiClO_4$[5]	None[1] 76.6[2]	None[1] 81.5[2]	None[1] 80.2[2]	None[1] 69.9[2]	None[1] 57.7[2]	None[1] 46.6[2]	n/d[6]	n/d[6]	n/d[6]	n/d[6]	n/d[6]
Duplex-Dark (**Fluorescein-G4** and **G4Comp-Quencher**)/$LiClO_4$[5]	None[1] 79.8[2]	None[1] 84.5[2]	None[1] 82.9[2]	None[1] 72.7[2]	None[1] 62.6[2]	None[1] 50.2[2]	n/d[6]	n/d[6]	n/d[6]	n/d[6]	n/d[6]

[1]G-Quadruplex unfolding

[2]Duplex unfolding

[3]Unfolding transition not complete at 95 °C so sigmoid fit not possible, number reported obtained using first derivative method where possible

[4]Folding transition not complete at 20 °C

[5]Only duplex-single stranded transition is observed in this system due to the absence of sodium and reporters used.

[6]Not determined owing to the lower solubility of $LiClO_4$ vs. $NaClO_4$

References Cited

1. Moore, G. E. Cramming More Components onto Integrated Circuits. *Electronics* **114-117**, (1965).
2. Waldrop, M. M. The chips are down for Moore's law. *Nature News* **530**, 144 (2016).
3. Morse, Mazor, Pohiman & Raveiel. Intel Microprocessors?8008 to 8086. **13**, 42–60 (1980).
4. Zafar, R. Apple A13 For iPhone 11 Has 8.5 Billion Transistors, Quad-Core GPU. *Wccftech* (2019). Available at: https://wccftech.com/apple-a13-iphone-11-transistors-gpu/. (Accessed: 25th September 2019)
5. Nenni, D. Samsung vs TSMC 7nm Update - Semiwiki. *Semiwiki* (2019). Available at: https://semiwiki.com/semiconductor-manufacturers/samsung-foundry/7926-samsung-vs-tsmc-7nm-update/. (Accessed: 25th September 2019)
6. Neisser, M. & Wurm, S. ITRS lithography roadmap: 2015 challenges. *Advanced Optical Technologies* **4**, 9425 (2015).
7. Wang, Y., Tang, Z., Tan, S. & Kotov, N. A. Biological assembly of nanocircuit prototypes from protein-modified CdTe nanowires. *Nano Lett.* **5**, 243–248 (2005).
8. Nishinaka, T. *et al.* Conductive metal nanowires templated by the nucleoprotein filaments, complex of DNA and RecA protein. *J. Am. Chem. Soc.* **127**, 8120–8125 (2005).
9. Reguera, G. *et al.* Extracellular electron transfer via microbial nanowires. *Nature* **435**, 1098–1101 (2005).
10. Wildt, B., Mali, P. & Searson, P. C. Electrochemical template synthesis of multisegment nanowires: fabrication and protein functionalization. *Langmuir* **22**, 10528–10534 (2006).
11. Vecchioni, S. *et al.* Construction and characterization of metal ion-containing DNA nanowires for synthetic biology and nanotechnology. *Sci. Rep.* **9**, 6942 (2019).
12. Beaucage, S. L. & Caruthers, M. H. Deoxynucleoside phosphoramidites—A new class of key intermediates for deoxypolynucleotide synthesis. *Tetrahedron Lett.* **22**, 1859–1862 (1981).
13. Kanvah, S. *et al.* Oxidation of DNA: damage to nucleobases. *Acc. Chem. Res.* **43**, 280–287 (2010).

14. Travascio, P., Li, Y. & Sen, D. DNA-enhanced peroxidase activity of a DNA-aptamer-hemin complex. *Chem. Biol.* **5**, 505–517 (1998).
15. Sen, D. & Poon, L. C. H. RNA and DNA complexes with hemin [Fe(III) heme] are efficient peroxidases and peroxygenases: how do they do it and what does it mean? *Crit. Rev. Biochem. Mol. Biol.* **46**, 478–492 (2011).
16. Golub, E., Freeman, R. & Willner, I. A hemin/G-quadruplex acts as an NADH oxidase and NADH peroxidase mimicking DNAzyme. *Angew. Chem. Int. Ed Engl.* **50**, 11710–11714 (2011).
17. Dawson, J. H. Probing structure-function relations in heme-containing oxygenases and peroxidases. *Science* **240**, 433–439 (1988).
18. Guo, J. U. & Bartel, D. P. RNA G-quadruplexes are globally unfolded in eukaryotic cells and depleted in bacteria. *Science* **353**, (2016).
19. Yang, S. Y. *et al.* Transcriptome-wide identification of transient RNA G-quadruplexes in human cells. *Nat. Commun.* **9**, 4730 (2018).
20. Chen, M. C. *et al.* Structural basis of G-quadruplex unfolding by the DEAH/RHA helicase DHX36. *Nature* **558**, 465–469 (2018).
21. Yurke, B., Turberfield, A. J., Mills, A. P., Jr, Simmel, F. C. & Neumann, J. L. A DNA-fuelled molecular machine made of DNA. *Nature* **406**, 605–608 (2000).
22. Alberti, P. & Mergny, J.-L. DNA duplex-quadruplex exchange as the basis for a nanomolecular machine. *Proc. Natl. Acad. Sci. U. S. A.* **100**, 1569–1573 (2003).
23. Liu, D. & Balasubramanian, S. A proton-fuelled DNA nanomachine. *Angew. Chem. Int. Ed Engl.* **42**, 5734–5736 (2003).
24. Bishop, J. D. & Klavins, E. An improved autonomous DNA nanomotor. *Nano Lett.* **7**, 2574–2577 (2007).
25. Wang, C., Huang, Z., Lin, Y., Ren, J. & Qu, X. Artificial DNA nano-spring powered by protons. *Adv. Mater.* **22**, 2792–2798 (2010).

26. Shao, C., Lu, N. & Sun, D. A G□Quadruplex/Hemin Complex with Switchable Peroxidase Activity by DNA Hybridization. *Chin. J. Chem.* **30**, 1575–1581 (2012).
27. Pegram, L. M. *et al.* Why Hofmeister effects of many salts favor protein folding but not DNA helix formation. *Proc. Natl. Acad. Sci. U. S. A.* **107**, 7716–7721 (2010).
28. Hud, N. V., Smith, F. W., Anet, F. A. & Feigon, J. The selectivity for K+ versus Na+ in DNA quadruplexes is dominated by relative free energies of hydration: a thermodynamic analysis by 1H NMR. *Biochemistry* **35**, 15383–15390 (1996).
29. Selvin, P. R. The renaissance of fluorescence resonance energy transfer. *Nat. Struct. Biol.* **7**, 730–734 (2000).
30. Moreira, B. G., You, Y., Behlke, M. A. & Owczarzy, R. Effects of fluorescent dyes, quenchers, and dangling ends on DNA duplex stability. *Biochem. Biophys. Res. Commun.* **327**, 473–484 (2005).
31. Salis, A. & Ninham, B. W. Models and mechanisms of Hofmeister effects in electrolyte solutions, and colloid and protein systems revisited. *Chem. Soc. Rev.* **43**, 7358–7377 (2014).
32. Zhou, M., Diwu, Z., Panchuk-Voloshina, N. & Haugland, R. P. A stable nonfluorescent derivative of resorufin for the fluorometric determination of trace hydrogen peroxide: applications in detecting the activity of phagocyte NADPH oxidase and other oxidases. *Anal. Biochem.* **253**, 162–168 (1997).
33. Semiconductor, F. 2N2369 Transistor. *Datasheet* (1984).
34. Tomiyasu, H. *et al.* An aqueous electrolyte of the widest potential window and its superior capability for capacitors. *Sci. Rep.* **7**, 45048 (2017).
35. Bu, X., Su, L., Dou, Q., Lei, S. & Yan, X. A low-cost 'water-in-salt' electrolyte for a 2.3 V high-rate carbon-based supercapacitor. *J. Mater. Chem. A Mater. Energy Sustain.* **7**, 7541–7547 (2019).
36. Kim, J. H. *et al.* Iron (II/III) perchlorate electrolytes for electrochemically harvesting low-grade thermal energy. *Sci. Rep.* **9**, 8706 (2019).
37. 2018 Semiconductor Synthetic Biology Roadmap.
38. biopharma-reporter.com. Agilent expands oligonucleotide manufacturing services. *biopharma-*

reporter.com (2009). Available at: https://www.biopharma-reporter.com/Article/2009/05/11/Agilent-expands-oligonucleotide-manufacturing-services. (Accessed: 26th September 2019)

39. Balasubramanian, S., Hurley, L. H. & Neidle, S. Targeting G-quadruplexes in gene promoters: a novel anticancer strategy? *Nat. Rev. Drug Discov.* **10**, 261–275 (2011).
40. Khatter, H., Myasnikov, A. G., Natchiar, S. K. & Klaholz, B. P. Structure of the human 80S ribosome. *Nature* **520**, 640–645 (2015).
41. Natchiar, S. K., Myasnikov, A. G., Kratzat, H., Hazemann, I. & Klaholz, B. P. Visualization of chemical modifications in the human 80S ribosome structure. *Nature* **551**, 472–477 (2017).
42. Mestre-Fos, S. *et al.* G-Quadruplexes in Human Ribosomal RNA. *J. Mol. Biol.* **431**, 1940–1955 (2019).
43. Drygin, D. *et al.* Quarfloxin (CX-3543) disrupts the Nucleolin/ rDNA quadruplex complexes, inhibits the elongation by RNA Polymerase I and exhibits potent antitumor activity in models of cancer. *Cancer Res.* **68**, 3301–3301 (2008).
44. O'Day, E. *et al.* An RNA-binding Protein, Lin28, Recognizes and Remodels G-quartets in the MicroRNAs (miRNAs) and mRNAs It Regulates. *J. Biol. Chem.* **290**, 17909–17922 (2015).
45. Mendoza, O., Bourdoncle, A., Boulé, J.-B., Brosh, R. M., Jr & Mergny, J.-L. G-quadruplexes and helicases. *Nucleic Acids Res.* **44**, 1989–2006 (2016).
46. Honda, K. *et al.* Ribosomal RNA in Alzheimer disease is oxidized by bound redox-active iron. *J. Biol. Chem.* **280**, 20978–20986 (2005).
47. Anger, A. M. *et al.* Structures of the human and Drosophila 80S ribosome. *Nature* **497**, 80–85 (2013).
48. Bonfio, C. *et al.* Prebiotic iron–sulfur peptide catalysts generate a pH gradient across model membranes of late protocells. *Nature Catalysis* **1**, 616–623 (2018).
49. Kim, J. D. *et al.* Minimal Heterochiral de Novo Designed 4Fe-4S Binding Peptide Capable of Robust Electron Transfer. *J. Am. Chem. Soc.* **140**, 11210–11213 (2018).

50. Muchowska, K. B., Varma, S. J. & Moran, J. Synthesis and breakdown of universal metabolic precursors promoted by iron. *Nature* **569**, 104–107 (2019).